

A stacked analysis of brightest cluster galaxies observed with the *Fermi* Large Area Telescope

K. L. Dutson,¹* R. J. White,¹ A. C. Edge,² J. A. Hinton¹ and M. T. Hogan²

¹*Department of Physics and Astronomy, The University of Leicester, University Road, Leicester LE1 7RH*

²*Department of Physics, Durham University, South Road, Durham DH1 3LE*

Accepted 2012 November 22. Received 2012 November 22; in original form 2012 September 14

ABSTRACT

We present the results of a search for high-energy γ -ray emission from a large sample of galaxy clusters sharing the properties of three existing *Fermi* Large Area Telescope detections (in Perseus, Virgo and A3392), namely a powerful radio source within their brightest cluster galaxy (BCG). From a parent, X-ray flux-limited sample of 863 clusters, we select 114 systems with a core-dominated BCG radio flux above 50/75 mJy (in the National Radio Astronomy Observatory Very Large Array Sky Survey and the Sydney University Molonglo Sky Survey, respectively), stacking data from the first 45 months of the *Fermi* mission in three energy bands, to determine statistical limits on the γ -ray fluxes of the ensemble of candidate sources.

For a >300 MeV selection, the distribution of detection significance across the sample is consistent with that across control samples for significances $<3\sigma$, but has a tail extending to higher values, including three $>4\sigma$ signals which are not associated with previously identified γ -ray emission. Modelling of the data in these fields results in the detection of four non-2FGL *Fermi* sources, though none of these appear to be *unambiguously* associated with the BCG candidate. Only one is sufficiently close to be a plausible counterpart (RXC J0132.6–0804) and the remaining three appear to be background active galactic nuclei. A search at energies >3 GeV hints at emission from the BCG in A2055, which hosts a BL Lac object.

There is no evidence for a signal in the stacked data, and the upper limit derived on the γ -ray flux of an average radio-bright BCG in each band is at least an order of magnitude more constraining than that calculated for individual objects. $F_{1\text{ GeV}}/F_{1.4\text{ GHz}}$ for an average BCG in the sample is <15 , compared with ≈ 120 for NGC 1275 in Perseus, which might indicate a special case for those objects detected at high energies. The tentative suggestion that point-like *beamed* emission from member galaxies comprise the dominant bright γ -ray sources in clusters implies searches for evidence of dark matter annihilation or large-scale merger shock signatures, for example, need to account for a significant level of contamination from within each cluster that is both highly stochastic and varies significantly over time.

Key words: radiation mechanisms: non-thermal – galaxies: active – galaxies: clusters: general – gamma-rays: galaxies: clusters – radio continuum: general.

1 INTRODUCTION

Feedback from the central active galactic nucleus (AGN) within a cooling-core cluster of galaxies is considered to play an integral large-scale role in the suppression of the observed cooling flow (see e.g. Fabian et al. 2002; Bower et al. 2006; Sijacki et al. 2007). The hot, diffuse, intracluster gas, which comprises 90 per cent of the baryonic matter of the cluster and is bound gravitationally by a cold dark matter (DM) halo, is revealed observationally through

thermal bremsstrahlung emission in the X-ray band. From velocity dispersion measurements, the atmosphere of this intracluster medium (ICM) typically has a temperature between 10^7 and 10^8 K (McNamara & Nulsen 2007). The gas loses energy to radiation primarily in the X-ray band, condensing on to the central galaxy, and subsonic, pressure-driven inflows develop within the dense cooling region, where the radiative cooling time for such emission, t_{cool} , is less than the age of the system (Fabian 1994).

However, as evidenced by spectroscopic data from current-generation X-ray observatories *Chandra* and *XMM-Newton*, emission predicted by the standard cooling-flow model from expected quantities of cooling gas is not detected (Peterson et al. 2003).

*E-mail: kate.dutson@leicester.ac.uk

This soft X-ray deficit necessitates some reheating mechanism that acts to replenish the energy being radiated away, thus quenching the cooling flow. An attractive agent for this feedback is the central AGN, whose outbursts would not only resolve the dearth of X-ray luminosity, but also account for the measured truncation at the high-mass end of the galaxy luminosity function (Benson et al. 2003).

Support for this explanation is given by high-resolution observations of cavities in the X-ray halo of many systems (e.g. Fabian et al. 2000; McNamara et al. 2000), coincident with radio synchrotron emission associated with the activity of the central engine. The AGN in the brightest cluster galaxy (BCG) injects energy into the ICM in the form of bubbles containing relativistic particles, which displace the thermal gas. So-called ‘ghost cavities’ have also been found using *Chandra*, interpreted as relics of past AGN activity: bubbles that have been previously detached from the radio lobes and risen buoyantly through the ICM and are no longer bright at 1.4 GHz. They are now known to be filled with *low-frequency* radio synchrotron emission (e.g. Clarke et al. 2005; Wise et al. 2007). This evidence implicates AGN outbursts as intermittent phenomena; the power output averaged over time of the central engine is able to balance the radiative cooling of the cluster core. For a review of AGN heating in clusters of galaxies, see McNamara & Nulsen (2007).

Both models of galaxy formation/clustering, and of feedback, and observations (including those aforementioned in the hard X-ray and radio bands) establish galaxy clusters as hosts to significant non-thermal particle populations (Völk & Atoyan 1999; Blasi, Gabici & Brunetti 2008). The remaining tracer of cosmic ray (CR) acceleration is γ radiation, and several emission scenarios predict BCGs to be sources of high-energy (HE) and very-high-energy (VHE) photons, with spectra dependent on the dominant energy content of the AGN jets: the nature of the seed particles they inject into the ICM, the strength of the local magnetic field, and the target density around the inflated bubbles (e.g. Hinton, Domainko & Pope 2007).

Ultra-relativistic particles may play an important role on several different scales in and around BCGs in cooling-core clusters, for example in AGN jets, mini haloes and cluster-scale haloes. γ -ray emission may arise in each via a number of dissimilar processes (e.g. Pfrommer & Enßlin 2004). Primary CR electrons accelerated in jets or re-accelerated fossil CRs in mini haloes will produce inverse Compton (IC) emission. Inelastic proton–proton collisions of *hadronic* CRs on the target medium will lead to π^0 decay emission and IC emission from secondary (or cascade) (e.g. Blasi & Colafrancesco 1999; Aharonian 2002) electrons. Most of these BCG-driven processes will produce GeV emission that is point-like for current detectors. However, it should be noted that – being massive and DM-dominated – clusters of galaxies are expected sources of *extended* γ -ray emission via DM annihilation (Ackermann et al. 2010a). Similarly, treating galaxy clusters as long-term reservoirs of CR hadrons, diffuse HE emission from π^0 decay of particles accelerated e.g. in cluster-scale accretion shocks is theorized (e.g. Pfrommer & Enßlin 2004). The various emission scenarios produce different spectral, temporal and spatial signatures at GeV energies. The repository of HE data afforded by the *Fermi Gamma-ray Space Telescope* (*Fermi*), since its launch in 2008, is therefore an attractive resource when used in conjunction with multiwavelength data. Whilst a detection of extended cluster emission at GeV energies is yet to be made (Ackermann et al. 2010b), point-like emission from a number of BCGs is seen and there is considerable potential for improving our understanding of this class of objects using GeV data.

To date, excluding systems whose AGN jets are favourably aligned close to the observer’s line of sight so as to boost emission via relativistic beaming – associated with ‘BL Lac’ objects within the *unified model* of active galaxies (Antonucci 1993) – only two BCGs have been confirmed as emitters of HE γ -rays. These are NGC 1275 and M87 (Abdo et al. 2009a,b), the dominant member galaxies of the cooling-core clusters Perseus and Virgo, respectively. Both are known to host bright central radio sources associated with the active nucleus (see Biretta, Stern & Harris 1991; Vermeulen, Readhead & Backer 1994; Sparks, Biretta & Macchetto 1996; Asada et al. 2006), and are also detected at VHEs (Aharonian et al. 2006; Aleksić et al. 2012). The multiwavelength emission of AGN is characteristically variable, and indeed the γ -ray flux is found to vary on time-scales down to days in the case of NGC 1275 (Brown & Adams 2011); similarly for M87 (Abramowski et al. 2012). Light-crossing-time arguments thus restrict the physical size of the emitting region responsible for, at least a component of, the γ -ray emission.

These sources are HE laboratories for the class of BCGs, and motivate a search for further instances of γ -ray activity within it. The purpose of this work is to conduct such a search, using data from the Large Area Telescope (LAT) on-board the *Fermi* satellite, accumulated thus far over the mission lifetime. To this end, we set out to imitate a deeper observation than is currently achievable in HE γ -rays given the sensitivity of the *Fermi*-LAT, by constructing a sample of many potential sources within the BCG class, and stacking the output of individual analyses.

We defend our derivation of a suitable sample of candidate sources in Section 2, and the *Fermi*-LAT analysis procedure then carried out for each target is described in Section 3. The results are presented in Section 4 and discussed in Section 5. Conclusions of the work are then drawn in Section 6.

2 TARGET SELECTION

Considering NGC 1275 to be prototypical of γ -ray sources within the class of BCGs, our selection criteria were therefore designed to identify similar objects. The key requirements were the presence of a massive cluster of galaxies and evidence of non-thermal activity in the BCG. We constructed a sample of candidates drawn from five parent catalogues of X-ray flux-limited galaxy clusters: the Brightest 55 (B55) Sample (Edge et al. 1990), the *ROSAT* Bright Cluster Sample (BCS; Ebeling et al. 1998), the extended *ROSAT* Bright Cluster Sample (eBCS; Ebeling et al. 2000), the *ROSAT*-ESO Flux-Limited X-ray (REFLEX) Galaxy Cluster Survey Catalogue (Böhringer et al. 2004) and the MAssive Cluster Survey (MACS; Ebeling, Edge & Henry 2001), encompassing objects from both the Southern and Northern hemispheres and including the brightest clusters from low Galactic latitudes. We include two clusters (RXC J1350.3+0940 and RXC J1832.5+6848) that meet the eBCS flux limit but were misidentified as AGN when the sample was published, due to the presence of a bright radio source, and for comparison, two X-ray-luminous clusters that contain known AGN [4C+55.16 (Hlavacek-Larrondo et al. 2011) and E 1821+643 (Russell et al. 2010)] though the cluster emission falls just below the eBCS limit once the AGN contribution is taken into account.

From this sample of 863 unique clusters (accounting for the small overlap between these five samples), we selected the 151 systems in which the BCG is detected above 50 mJy in the National Radio Astronomy Observatory (NRAO) Very Large Array (VLA) Sky Survey (NVSS; Condon et al. 1998) or 75 mJy in the Sydney University Molonglo Sky Survey (SUMSS; Mauch et al. 2003). We took care to

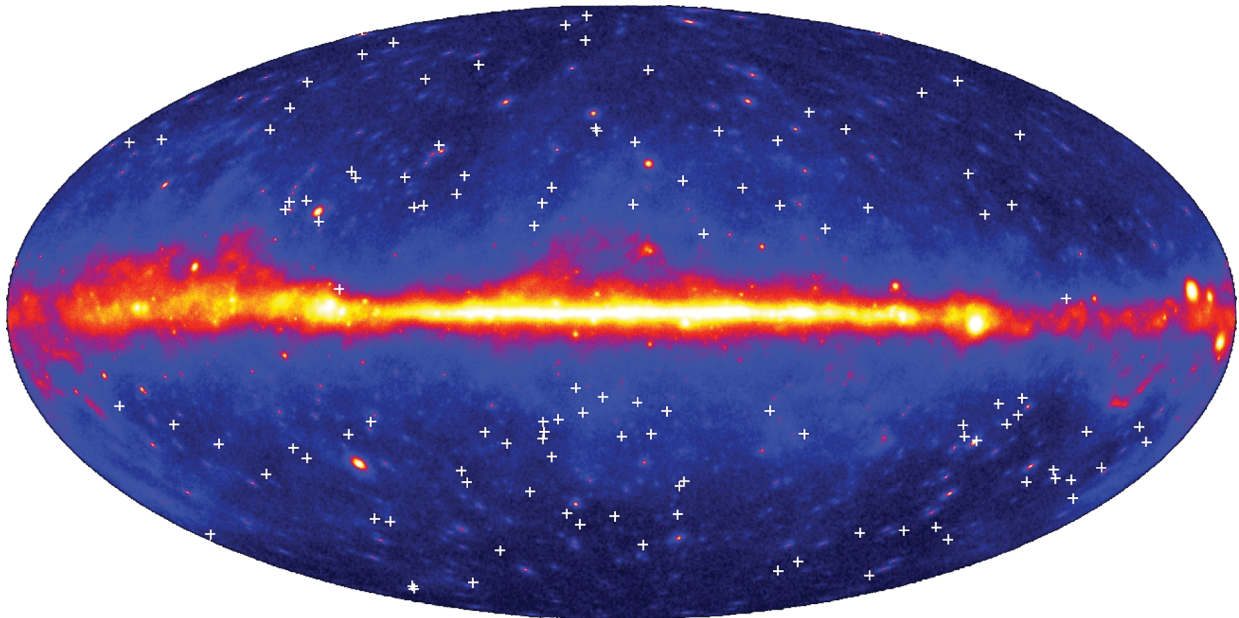


Figure 1. An all-sky map constructed from ~ 45 months of $300 \text{ MeV} \leq E \leq 300 \text{ GeV}$ *Fermi* data, scaled logarithmically. The BCG positions of the 114 candidates of the main sample are indicated by the white crosses.

remove systems where the radio emission is from a cluster member projected close to the BCG. Of this sample we have higher resolution radio imaging from the VLA or Australia Telescope Compact Array (ATCA) at 5 and/or 8 GHz for the majority (114 of 151), which can be used to identify those sources with a significant, flat spectrum core component (Hogan et al., in preparation).

We have optical spectra for 148 of the 151 BCGs recognized by our radio selection, and of these 64 per cent (97 objects) exhibit optical line emission. This is significantly higher than the 25–30 per cent of the BCGs in an X-ray selected sample presenting line emission, indicating that our radio selection strongly prefers clusters with a cooling flow (Burns 1990; Cavagnolo et al. 2008; Mittal et al. 2009; Hogan et al., in preparation).

The sample represents a complete selection of radio-bright clusters that is dominated by cooling-core clusters, spanning a wide range in redshift ($0.009 < z < 0.45$). It can be divided into BCGs whose radio emission has some contribution from the core or is core-dominated, and those with extended radio morphology and a lobe-dominated radio flux. The former comprise 114 objects and constitute the ‘main sample’ (see Fig. 1 and Table 1), with the remaining 37 BCGs forming an ‘extended sample’. We compiled a counter sample of 65 ‘control’ clusters drawn from the parent X-ray sample that do *not* contain a radio-bright BCG, or optical emission lines, but share the same redshift distribution as the radio-bright sample for a representative comparison. We also generated a pair of control samples of 114 candidate sources each with random positions on the sky (generated by performing first a positive and then a negative 5° shift in Galactic latitude on the coordinates of the main sample candidates) for direct comparison with the main sample.

The parent clusters of the main sample BCGs include hosts to five BL Lac objects, two of which are known HE γ -ray sources listed in the *Fermi*-LAT Second Source Catalog (2FGL; Nolan et al. 2012): 2FGL J0627.1–3528 in A3392 and 2FGL J1958.4–3012 in RXC J1958.2–3011. The other three BL Lacs, RGB J1144+676 in A1366, RGB J1518+062 in A2055 and B2 2334+23 in A2627, are not known *Fermi* sources. These BL Lacs are included as the original cluster identification from the *ROSAT* Survey incor-

rectly attributed the (bulk of the) X-ray emission to the cluster (e.g. RXC J1958.2–3011; Böhringer et al. 2004). However, in all five cases, pointed *Chandra* or *XMM-Newton* observations indicate that the BL Lac dominates the emission, so the cluster does not meet the X-ray flux limit applied to select the other clusters. Therefore, even this small *Fermi*-LAT detection fraction is an upper limit, given only NGC 1275 (a misaligned blazar) and M87 (a radio galaxy) are dominated by the extended X-ray emission from their host cluster, and hence meet the cluster selection criteria. For the purpose of the analyses detailed hereafter, these two well-studied BCGs are not included in the sample, since our aim is to identify whether any additional sources in the class are detected using *Fermi*. There is no *clear* cluster around RXC J1958.2–3011, so its classification as a BCG is not certain, but with this caveat in mind it is kept, particularly as an additional *Fermi* source to check the output of analyses against.

3 *Fermi*-LAT OBSERVATIONS AND DATA ANALYSIS

The *Fermi*-LAT is a pair conversion instrument sensitive to photons of energy ~ 20 MeV to >300 GeV, with a wide field of view (2.4 sr) and large effective area ($\approx 8000 \text{ cm}^2$ on-axis at 1 GeV). The detector is described in detail in Atwood et al. (2009, and references therein). *Fermi* observations are taken primarily in *all-sky-survey* mode, in which the spacecraft is pointed at some angle from the zenith, and rocked north and south of its orbital plane, scanning the whole sky every ~ 3 h.

The 151 BCGs of our main and extended samples were treated as candidate point sources of HE γ -rays, and each analysed using the *Fermi* Science Tools version v9r27p1, and instrument response function (IRF) P7SOURCE_V6. Event and spacecraft *all-sky-survey* data amassed between 2008 August 4 and 2012 April 28 (a Mission-Elapsed-Time interval of 239 557 417 to 357 308 125, equating to ~ 1362 d) were extracted for a source region (SR) of 12° , centred on each BCG position (taken from optical data in the literature) and in the energy range $300 \text{ MeV} \leq E \leq 300 \text{ GeV}$ [thus

Table 1. A summary of the 114 BCGs of the main sample, and their candidate *Fermi* source properties, including the upper limit on the γ -ray flux above 300 MeV. The radio emission is classified as core-dominated ('c'), extended-with-core-contribution ('e') or BL Lac-associated ('b').

Parent cluster	l^a ($^\circ$)	b^b ($^\circ$)	z	1.4 GHz ^c radio flux (mJy)	TS ^d	γ -ray flux upper limit (ph cm ⁻² s ⁻¹)
RXC J0000.1+0816	101.9	-52.5	0.04	84 c	0	2.2×10^{-10}
A85	115.3	-72.0	0.056	58 c	0	2.8×10^{-10}
Z235	120.8	-38.4	0.083	50 c	3.2	5.7×10^{-10}
3C 31	126.9	-30.3	0.016	1108 e	2.2	5.8×10^{-10}
RXC J0132.6-0804	152.0	-68.6	0.15	308 c	24.0	1.6×10^{-9}
MACS J0242.5-2132	206.6	-64.1	0.31	1255 c	0	1.9×10^{-10}
A3112	253.0	-56.1	0.075	1915 c	11.2	8.2×10^{-10}
A496	209.7	-36.5	0.033	121 c	5.8	9.2×10^{-10}
RXC J0439.0+0520	191.4	-26.2	0.21	82 c	6.0	8.2×10^{-10}
NGC 1650	214.0	-34.9	0.036	91 c	0	5.0×10^{-10}
S555	243.6	-26.3	0.044	319 c	0	2.1×10^{-10}
A3378	241.9	-24.0	0.14	1337 c	0	2.9×10^{-10}
A3392	243.5	-20.0	0.055	4513 b	221.0	-
PKS 0745-191	236.5	3.0	0.1	2373 c	13.7	8.2×10^{-10}
A646	172.7	34.6	0.13	54 c	0	8.3×10^{-11}
4C+55.16	162.3	36.6	0.24	8284 c	1.6	4.9×10^{-10}
Hydra-A	243.0	25.1	0.054	40850 c	2.7	4.8×10^{-10}
MACS J1133.2+5008	150.7	62.6	0.39	846 e	0	2.3×10^{-10}
A1348	277.4	47.1	0.12	158 c	0	1.4×10^{-10}
A1366	132.6	48.5	0.12	237 b	0	3.0×10^{-10}
NGC 4696	302.5	21.6	0.0098	5674 e	0	3.4×10^{-10}
MACS J1347.5-1145	324.1	48.8	0.45	48 c	43.4	-
A1795	33.9	77.2	0.062	925 e	0	1.9×10^{-10}
RXC J1350.3+0940	344.3	67.7	0.13	293 c	0	1.0×10^{-10}
A3581	323.2	32.9	0.023	646 c	7.4	1.1×10^{-9}
A1885	83.2	66.6	0.089	49 c	0	1.2×10^{-10}
S780	341.0	35.1	0.24	106 c	1.5	3.1×10^{-10}
RXC J1504.1-0248	355.1	46.2	0.22	62 c	7.3	9.6×10^{-10}
A2052	9.5	50.1	0.035	5500 c	0	2.4×10^{-10}
A2055	8.9	49.3	0.1	498 b	8.0	8.4×10^{-10}
RXC J1524.2-3154	337.1	20.7	0.1	50 c	2.0	5.3×10^{-10}
RXC J1558.3-1410	356.6	28.7	0.097	461 c	1.7	6.8×10^{-10}
A2199	63.0	43.7	0.03	3681 e	1.5	5.9×10^{-10}
NGC 6338	85.9	35.4	0.028	57 c	0	3.5×10^{-10}
Z8193	67.6	34.7	0.18	134 c	0	2.7×10^{-10}
A2270	83.1	33.8	0.24	144 c	2.6	5.1×10^{-10}
Z8276	58.0	27.6	0.076	92 c	0	5.6×10^{-10}
RXC J1750.2+3504	60.6	27.0	0.17	69 c	0	1.5×10^{-10}
E1821+643	94.1	27.4	0.3	94 e	1.3	2.7×10^{-10}
RXC J1832.5+6848	99.2	26.8	0.2	150 c	0	1.1×10^{-10}
A3639	347.0	-26.3	0.15	139 c	0	2.1×10^{-10}
RXC J1931.6-3354	5.2	-22.5	0.097	886 c	0	2.8×10^{-10}
MACS J1931.6-2634	12.6	-20.1	0.35	223 c	7.4	1.0×10^{-9}
RXC J1958.2-3011	11.0	-26.8	0.12	128 b	46.3	-
Cyg-A	76.3	5.8	0.056	1590000 e	4.5	7.9×10^{-10}
S851	351.0	-32.6	0.0097	139 c	0	9.3×10^{-10}
RXC J2014.8-2430	18.4	-28.5	0.16	230 e	0	3.4×10^{-10}
A2390	74.0	-27.8	0.23	236 c	11.2	4.3×10^{-10}
RXC J2213.1-2754	22.3	-55.0	0.061	76 c	0	2.8×10^{-10}
A3880	18.1	-58.5	0.058	228 c	4.0	5.7×10^{-10}
A2597	65.4	-64.9	0.085	1875 e	0	1.9×10^{-10}
A2627	101.8	-35.9	0.13	434 b	9.8	8.3×10^{-10}
A2634	103.6	-33.1	0.03	1037 e	0	1.9×10^{-10}
RXC J0137.2-0911	156.3	-69.1	0.041	178 e	0	3.1×10^{-10}

Table 1 – continued

Parent cluster	l^a (°)	b^b (°)	z	1.4 GHz ^c radio flux (mJy)	TS ^d	γ -ray flux upper limit (ph cm ⁻² s ⁻¹)
A262	136.6	-25.1	0.017	67 e	0	4.3×10^{-10}
A2984	256.6	-68.9	0.1	232 c	0	1.5×10^{-10}
A3017	256.6	-65.7	0.22	127 c	3.3	5.1×10^{-10}
Z808	175.4	-47.3	0.17	393 e	0	9.6×10^{-11}
A407	150.7	-19.9	0.048	661 c	0	1.7×10^{-10}
RXC J0331.1-2100	212.3	-53.2	0.19	168 c	0	2.5×10^{-10}
NGC 1399	236.8	-53.6	0.0051	2500 e	2.9	4.8×10^{-10}
A3165	226.4	-51.4	0.14	921 c	0	1.4×10^{-10}
RXC J0359.1-0319	193.4	-39.3	0.12	188 e	0	2.8×10^{-10}
RXC J0425.8-0833	203.4	-36.2	0.04	112 e	0	2.5×10^{-10}
MACS J0429.6-0253	197.9	-32.6	0.4	139 c	0	1.3×10^{-10}
A499	218.5	-38.3	0.15	158 e	0	4.8×10^{-10}
RXC J0501.4+0110	198.5	-23.7	0.12	121 c	0	3.2×10^{-10}
MACS J0520.7-1328	215.3	-26.1	0.34	93 c	0	2.8×10^{-10}
A3360 ^e	249.4	-30.7	0.085	222 c	0	2.2×10^{-10}
S547	254.2	-30.0	0.051	143 e	0	3.1×10^{-10}
A3380	257.2	-27.3	0.055	1455 e	1.0	5.1×10^{-10}
A3396	250.0	-21.6	0.18	614 e	2.5	2.4×10^{-10}
A795	217.1	40.2	0.14	116 c	1.1	1.8×10^{-10}
S617	253.3	23.3	0.034	105 e	7.3	7.5×10^{-10}
A907	249.4	33.3	0.17	69 c	0	1.5×10^{-10}
A923	205.3	53.3	0.12	73 c	0	1.9×10^{-10}
Z3179	228.7	53.1	0.14	94 c	6.6	7.4×10^{-10}
Z3916	144.7	54.4	0.21	66 c	0	9.0×10^{-11}
A1361	153.4	66.6	0.12	864 e	0	3.0×10^{-10}
A3490	287.8	26.5	0.07	368 e	0	2.0×10^{-10}
A1412	128.4	43.1	0.083	73 e	0	2.0×10^{-10}
MACS J1206.2-0847	284.5	52.4	0.44	161 e	0	1.1×10^{-10}
A1644	305.0	45.4	0.047	98 c	0	5.8×10^{-10}
A1677	84.0	85.1	0.18	76 c	0	1.7×10^{-10}
NGC 5098	78.8	81.3	0.036	83 c	0	3.7×10^{-10}
A3565	313.6	28.0	0.012	3000 e	0	5.4×10^{-10}
MACS J1411.3+5212	97.6	60.8	0.46	22720 e	0	3.9×10^{-10}
A2204	21.2	33.2	0.15	70 c	0	1.3×10^{-10}
HerA	23.1	28.9	0.15	34000 e	3.6	3.3×10^{-10}
NGC 6269	49.1	35.9	0.035	51 c	3.0	2.5×10^{-10}
RXC J1715.1+0309	24.5	22.8	0.13	165 c	0	2.7×10^{-10}
RXC J1720.1+2637	49.3	30.9	0.16	89 e	0	1.4×10^{-10}
RXC J1840.6-7709	317.3	-25.8	0.019	1152 e	0	2.3×10^{-10}
RXC J1852.1+5711	87.1	22.4	0.11	51 c	0	4.5×10^{-10}
A2312	99.0	24.8	0.095	79 c	5.4	6.3×10^{-10}
A3638	355.4	-24.0	0.077	258 c	0	2.4×10^{-10}
IC 4991	359.9	-33.2	0.019	109 c	16.0	1.6×10^{-9}
S868	22.9	-29.1	0.056	229 c	0	2.1×10^{-10}
RXC J2034.9-2143	23.2	-32.0	0.19	82 c	0	3.4×10^{-10}
RXC J2043.2-2144	23.9	-33.8	0.2	295 e	0	1.8×10^{-10}
A2331	40.9	-31.7	0.079	106 e	5.3	3.5×10^{-10}
RXC J2101.5-1317	35.4	-34.8	0.028	1200 e	0	1.9×10^{-10}
RBS 1712	22.2	-38.8	0.19	67 c	0	1.9×10^{-10}
APM 699	338.1	-45.7	0.082	152 e	11.7	9.8×10^{-10}
RXC J2151.3-5521	339.2	-47.1	0.038	108 e	9.3	3.0×10^{-10}
A2384	33.4	-48.4	0.096	54 c	0	3.1×10^{-10}
A2389	53.7	-41.8	0.15	78 c	0	3.6×10^{-10}
A2415	54.0	-45.1	0.058	187 c	0	1.4×10^{-10}
A3856	2.8	-56.2	0.14	186 e	0	1.6×10^{-10}
A2445	83.0	-30.8	0.17	77 c	6.0	4.3×10^{-10}
A3911	336.7	-55.4	0.097	418 e	0	1.5×10^{-10}

Table 1 – *continued*

Parent cluster	l^a (°)	b^b (°)	z	1.4 GHz ^c radio flux (mJy)	TS ^d	γ -ray flux upper limit (ph cm ⁻² s ⁻¹)
S1101	348.4	−64.8	0.056	472 c	0	3.0×10^{-10}
A4023	304.7	−31.7	0.19	<i>143 e</i>	0	2.9×10^{-10}
A2665	97.0	−53.6	0.057	56 c	0	1.7×10^{-10}

^aGalactic longitude.^bGalactic latitude.^cTaken from the NVSS. If italicized, the values instead denote the 843 MHz radio flux taken from the SUMSS.^dTest Statistic – for clarity TS values <1 are shown as zero.^eDespite a low TS, this source was not included in the stacked analysis (see Section 4.2) due to the proximity of a bright 2FGL source, as detailed in the text.

discarding events at the lowest energies, where the high point spread function (PSF) results in considerable source confusion]. A zenith cut of 100° was applied to eliminate γ -rays from the Earth’s limb, and all ‘Source’ class events were considered.

For each candidate source the data were fitted to a source model constructed to describe (in addition to potential emission from the target BCG) the emission from nearby (i.e. within the SR) 2FGL sources and the diffuse Galactic and extragalactic (isotropic) γ -ray backgrounds (thus recent models `gal_2yearp7v6_v0.fits` and `iso_p7v6source.txt`, respectively,¹ were utilized; their normalization is free to vary). The photon index and normalization for objects within 1° of the candidate position were allowed to vary. Outside of this region but within the specified *region of interest* (ROI) of 8° , the normalization was free to vary, but the photon index was fixed to the 2FGL value. Sources outside of the ROI but within the SR were included in the model, but their aforementioned parameters were fixed to the catalogue values. In the event that a candidate position coincided with a 2FGL source (within 0.2°), then that source was automatically removed from the model. This action provides a useful check of the output of our analyses against the catalogue values for known *Fermi* sources, whilst allowing all BCGs in the sample to be treated in the same way.

The maximum-likelihood spectral estimator `GTLIKE` was used to perform a *binned* fit, modelling the candidate source emission with a power-law spectrum. `GTMODEL` was then used to obtain a model map of each candidate region given the result of the fit. To construct counts maps from the data, `GTBIN` was utilized. Binned exposure cubes were also generated (through the use of the `GTEXPCUBE2` tool) as part of the binned likelihood analysis chain. A binned method of likelihood fitting was adopted over an unbinned one because it was found to be more robust, with the fit converging irrespective of how many 2FGL sources a given SR contained.

The distribution of Test Statistic (TS) values (output by `GTLIKE`) across the sample could then be studied. A critical TS of 25 (corresponding roughly to a detection significance of 5σ ; Mattox et al. 1996) was decided upon, below which an upper limit on the source emission was automatically calculated. All candidate sources with $TS \gtrsim 16$ were nevertheless investigated on an individual basis: TS maps were constructed and any peaks found thereon were fitted with parabolic ellipsoids to localize the emission. Where appropriate the data were then remodelled to constrain potential new *offset* sources.

The ensemble of counts maps constructed from the sample data, and that of the model maps output from fitting based on a *null* hypothesis (i.e. the absence of a candidate *Fermi* source at the

position of the BCG), were stacked. These stacked maps could then be sliced to provide 1D comparisons between the summed model fit and the data. To derive an upper limit on the γ -ray flux of an average source in our sample using this stacking method, the stacked counts map was used to obtain a number of *on-source* counts (N_{on}) within a region of radius comparable with the PSF of the LAT instrument on average across the selected energy band. An estimate of the number of background photons in this region, \hat{N}_{B} , was obtained by similarly integrating the stacked model map. The number of *off-source* counts (N_{off}) is then $\hat{N}_{\text{B}}/\alpha$, where α is taken as the ratio of the solid angle in the chosen radius to that of the field of view. Thus, an estimate of the γ -ray signal present is given by the excess counts, $N_{\text{on}} - \alpha N_{\text{off}}$. A 95 per cent confidence upper limit on the signal was computed following the method of Rolke, López & Conrad (2005), assuming only Poisson errors on the background estimate. Whilst a more sophisticated likelihood method similar to that used by Huber et al. (2012) may provide a modest sensitivity improvement, our approach is simple and robust.

Weighted exposure maps were constructed for each candidate source and stacked, to provide a summed exposure map from which the exposure averaged over solid angle in the on-region could be determined. This value was used to transform our signal upper limit to an upper limit on the γ -ray flux. The rms variation in exposure across the sample is ≈ 6 per cent.

For the purpose of investigating potential weak, hard spectrum, candidate source emission (less contaminated by the diffuse background) and given that stacking is most promising in the signal-limited regime where every additional field adds potential source photons with minimal cost in background contamination, energy cuts above 3 and 30 GeV were applied to the data and the analyses repeated in an otherwise identical manner; upper limits calculated within regions of radii were comparable to the LAT PSF at the respective lower energy bounds. Corresponding analyses were performed simultaneously for the control and radio-quiet samples.

4 RESULTS

A summary of the source properties of the BCGs of the main sample, their respective TS values and/or upper limits output from the analysis procedure outlined in Section 3 is given in Table 1. For the sake of clarity, the test statistic is shown as zero for sources with $TS < 1$. An upper limit is included for sources with $TS < 25$. Those BCGs with $TS > 25$ are in A3392, RXC J1958.2–3011 and MACS J1347.5–1145.

As noted in Section 2, the sources in A3392 and RXC J1958.2–3011 correspond to the known *Fermi* sources 2FGL J0627.1–3528 and 2FGL J1958.4–3012, respectively. The

¹ <http://fermi.gsfc.nasa.gov/ssc/data/access/lat/BackgroundModels.html>

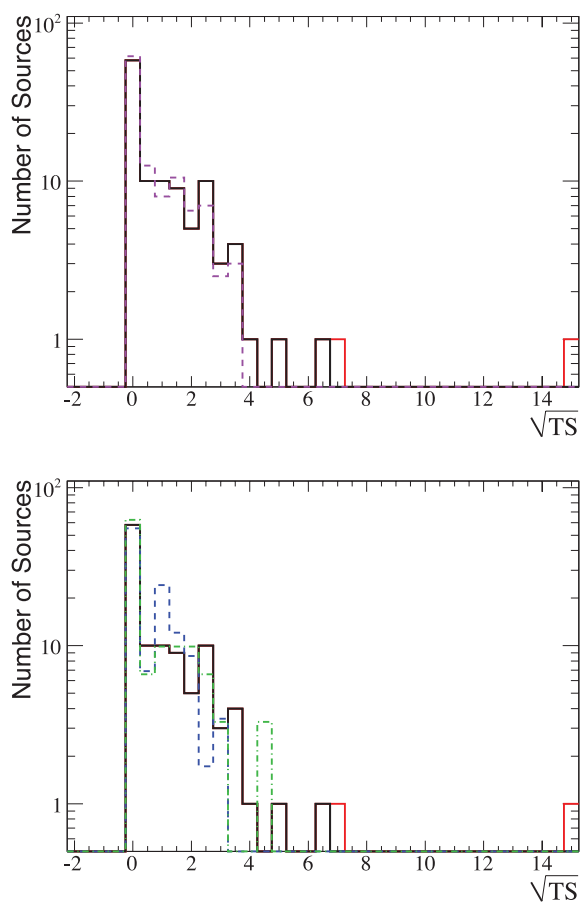


Figure 2. Histograms showing the comparison between the distribution of detection significance across the samples described in Section 2. The main sample of BCGs (black line) is included on both plots. Top panel: the (averaged) control sample of random positions on the sky (dashed violet line). Bottom panel: the scaled extended cluster sample (dot-dashed green line) and radio-quiet cluster sample (dashed blue line). The (two) sample BCGs with existing *Fermi* detections have been added in red.

BCG in MACS J1347.5–1145 is *not* in the 2FGL catalogue. These sources and those that fall shy of the TS cut, but for which TS is greater than ≈ 16 , are discussed in Section 4.3.

4.1 Distribution of detection significance

The distribution of $\sqrt{\text{TS}}$ (corresponding approximately to the statistical significance, see Section 3) for each sample analysed is shown in Fig. 2. The extended and radio-quiet cluster samples have been scaled appropriately, and the control samples averaged, so that comparisons may easily be made with the main sample of 114 objects. Common to all distributions is a clear peak at 0, and also a tail containing several signals at up to $\approx 3\sigma$. However, this tail is more pronounced for the main sample – implying that a stacking analysis may be worthwhile (see Section 4.2) – and outliers are present; the high-TS sources are visible above 4σ (see Section 4.3), including the two *Fermi* sources shown in red: all members of the main sample. The only exception is the extended sample BCG in S 753, for which a TS of 19.9 was derived. Inspection of the field containing this object reveals a highly confused region of diffuse emission, likely associated with the Galactic background, and as such this result is not believed.

4.2 Stacking analysis

The stacked analyses of the main sample above the three energy cuts – described in Section 3 – are illustrated in Fig. 3. In each case the left-hand panel shows the stacked counts map in the colour scale, overlaid with contours defining the corresponding stacked model map for the null hypothesis. The maps to be summed were each centred on the candidate source position (0,0), which is marked on the final stacked plot. The right-hand panels show 1D slices through both the summed counts and model maps (the area covered by these slices is indicated by the boxes drawn on the stacked maps; their width motivated in each case by the LAT PSF as described in Section 3, to match the regions within which upper limits are computed: 1° , 0.4 and 0.2 for the ≥ 300 MeV, ≥ 3 GeV and ≥ 30 GeV data sets, respectively). Sources with a high individual TS (> 16) and those within 0.2 of a catalogue source are not included in the stack. The field containing the BCG A3360 has also been removed, due to the proximity (within 1°) of the very bright $[(3.71 \pm 0.07) \times 10^{-8} \text{ ph cm}^{-2} \text{ s}^{-1}]$ 2FGL source 2FGL J0538.8–4405. The model provides a reasonable description of the data, and there is no evidence for an excess close to the origin. Applying the method described in Section 3, the derived 95 per cent upper limits on the γ -ray flux of an average source within the class of BCGs, given the cuts applied and within a region of size comparable with the LAT PSF, are found to be $7.4 \times 10^{-11} \text{ ph cm}^{-2} \text{ s}^{-1}$ (within a 1° radius for $300 \text{ MeV} \leq E \leq 300 \text{ GeV}$), $7.1 \times 10^{-12} \text{ ph cm}^{-2} \text{ s}^{-1}$ (within a 0.4 radius for $3 \leq E \leq 300 \text{ GeV}$) and $3.7 \times 10^{-13} \text{ ph cm}^{-2} \text{ s}^{-1}$ (within a 0.2 radius for $30 \leq E \leq 300 \text{ GeV}$).

4.3 Sources of note

4.3.1 2FGL sources

The *Fermi* source 2FGL J0627.1–3528 is associated with the BCG in A3392, which is classified as a BL Lac object. It is listed with a 24-month detection significance of 12.6, $100 \text{ MeV} \leq E \leq 100 \text{ GeV}$ flux of $(1.50 \pm 0.18) \times 10^{-9} \text{ ph cm}^{-2} \text{ s}^{-1}$ and photon index of 1.93 ± 0.09 . With 21 months more data (and in an energy band $300 \text{ MeV} \leq E \leq 300 \text{ GeV}$) we calculate an increased detection significance of 14.9, and a consistent (within errors) photon index, as expected.

The *Fermi* source 2FGL J1958.4–3012 is associated with the BL Lac object RXC J1958.2–3011, and may be a BCG (see Section 2). It is listed with a 24-month detection significance of 5.1, $100 \text{ MeV} \leq E \leq 100 \text{ GeV}$ flux of $(5.94 \pm 1.78) \times 10^{-10} \text{ ph cm}^{-2} \text{ s}^{-1}$ and photon index of 1.9 ± 0.2 . With 21 months more data (and in an energy band $300 \text{ MeV} \leq E \leq 300 \text{ GeV}$) we calculate an increased detection significance of 6.8, and a consistent (within errors) photon index, as expected.

4.3.2 Offset detections: possible counterparts

TS maps were constructed for candidate sources with $\text{TS} \gtrsim 16$ to better localize the source position. These can be seen in Fig. 4 for the BCGs in MACS J1347.5–1145 ($\text{TS} = 43.4$), RXC J0132.6–0804 ($\text{TS} = 24.0$) and IC 4991 ($\text{TS} = 16.0$), and illustrate the effect of neglecting to add the candidate to the model: significant sources are revealed and localized where the baseline model (containing all local 2FGL sources, and the diffuse Galactic and extragalactic backgrounds; see Section 3) fails to describe the γ -ray emission. These peaks in TS were fitted with parabolic ellipsoids and the best-fitting peak positions are illustrated in the figure. The contours

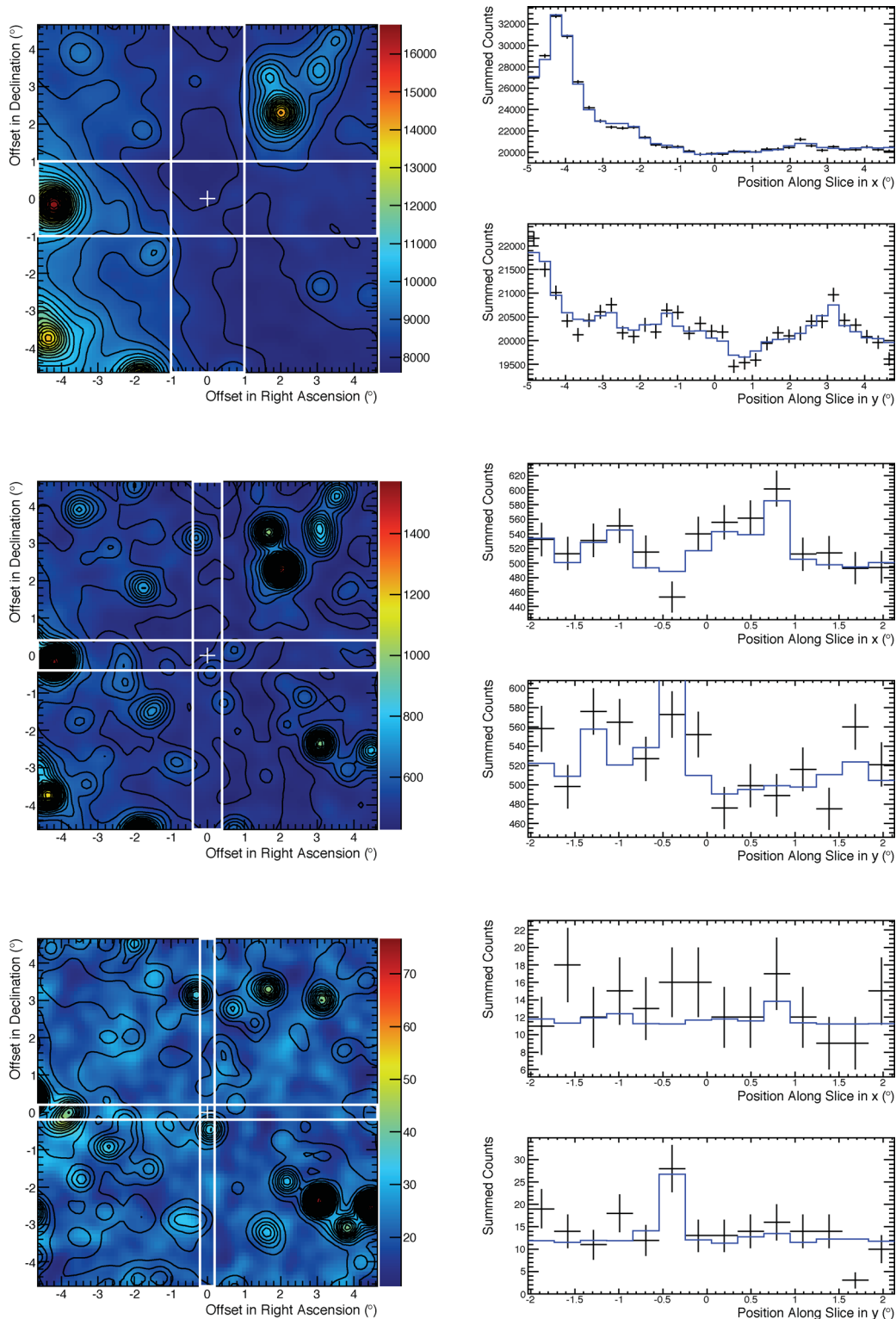


Figure 3. Stacked counts maps for the main sample of BCGs above an energy of 300 MeV (top), 3 GeV (middle) and 30 GeV (bottom), overlaid with contours representing the corresponding stacked model maps (for the null hypothesis). The white cross indicates the BCG position in all fields. The stacked maps have been smoothed with a Gaussian kernel of rms $0\text{.}2$. A cut in candidate source TS above 16 has been applied, and additionally a *proximity* cut of $0\text{.}2$ (to remove fields where the candidate position is coincident with a *Fermi*-LAT source). Neglecting also fields for which a 2FGL source brighter than $1 \times 10^{-8} \text{ ph cm}^{-2} \text{ s}^{-1}$ is found to be within 1° of the central position (see Section 4.2), these stacks then comprise 109 (top) and 111 (middle; bottom) individual fields. The boxed regions indicate the area of the slices (to the right of each stack) through both maps in the horizontal and vertical directions, allowing a 1D comparison between the data (black points) and null model (blue line).

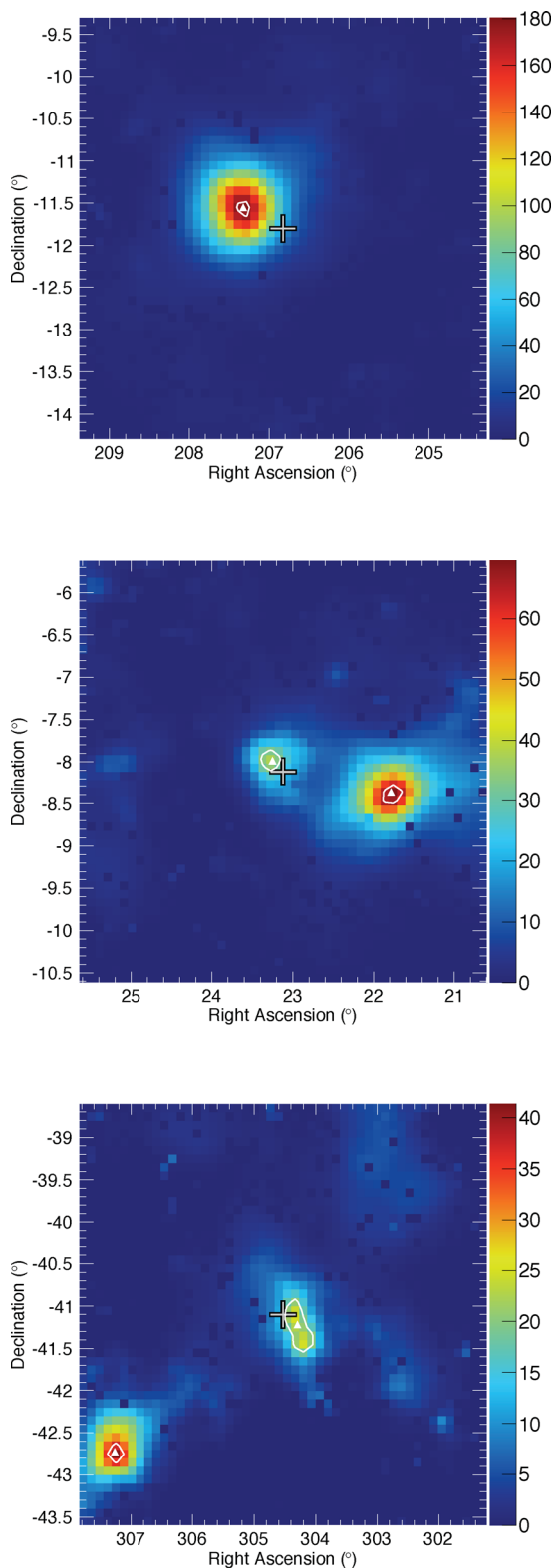


Figure 4. TS map for candidate sources in MACS J1347.5–1145 (top), RXC J0132.6–0804 (middle) and IC 4991 (bottom) produced from $300 \text{ MeV} \leq E \leq 300 \text{ GeV}$ data. The BCG position is indicated by the central black/grey cross. Peaks in TS have been fitted with parabolic ellipsoids, the fit position for which is shown by a white triangle and given in Table 2. The 95 per cent confidence contours on source locations are shown in white.

represent the 95 per cent confidence regions for the positions of the sources.

Adding a candidate at the position of the BCG in MACS J1347.5–1145 (in the energy band $300 \text{ MeV} \leq E \leq 300 \text{ GeV}$) yields a photon index of 2.76 ± 0.01 and a flux of $(3.81 \pm 0.70) \times 10^{-9} \text{ ph cm}^{-2} \text{ s}^{-1}$. The significant source in the field, however, is clearly offset from the BCG position [the fitted peak in TS is located at right ascension (RA) = $207^{\circ}33'$, declination (Dec.) = $-11^{\circ}55'$] and so unlikely to be associated. Consulting the literature reveals the *Fermi*-LAT detection of a GeV flare consistent (within the quoted statistical errors) with this location in 2011 November (Torresi & D’Ammando 2011, ATel 3788), and the flat-spectrum $z = 0.34$ quasi-stellar object (QSO) PKS 1346–112 (Jackson et al. 2002) is given as a possible counterpart. Following this detection, a possible *Wide-field Infrared Survey Explorer* (*WISE*) blazar counterpart was identified, coincident with the radio source (Paggi et al. 2012, ATel 4086). Re-running the likelihood analysis with this new source included in the model yields a negligible TS at the BCG position, and a TS of 179.6 (corresponding to a detection significance of $\approx 13.4\sigma$) at the peak position, with a corresponding photon index of 2.44 ± 0.03 and flux of $(3.04 \pm 0.15) \times 10^{-8} \text{ ph cm}^{-2} \text{ s}^{-1}$. Despite the high TS value, the transient nature of the source may account for its absence from the 2FGL.

Adding a candidate at the position of the BCG in RXC J0132.6–0804 (in the energy band $300 \text{ MeV} \leq E \leq 300 \text{ GeV}$) yields for the source a photon index of 2.20 ± 0.02 and a flux of $(1.42 \pm 0.50) \times 10^{-9} \text{ ph cm}^{-2} \text{ s}^{-1}$. There appear to be two significant sources in the field, the more central of which (the fitted TS peak is located at RA = $23^{\circ}25'$, Dec. = $-7^{\circ}98'$) is 8 arcmin from the BCG and may be associated with a member of the parent cluster. The most significant peak is fitted to a position at RA = $21^{\circ}78'$, Dec. = $-8^{\circ}37'$. The BL Lac FBQS J0127–0821 at a redshift of 0.36 is a plausible γ -ray counterpart (Plotkin et al. 2008). A re-analysis of the field using a model containing these two localized sources nullifies the BCG TS, and results in a TS of 28.0 for the closer peak, and 65.0 for the remaining one, corresponding to $\approx 5.3\sigma$ and $\approx 8\sigma$ detections, respectively. A photon index of 2.36 ± 0.03 and flux of $(1.14 \pm 0.06) \times 10^{-8} \text{ ph cm}^{-2} \text{ s}^{-1}$ is calculated for the latter, and for the former a photon index of 1.98 ± 0.03 , and a flux of $(3.06 \pm 0.24) \times 10^{-9} \text{ ph cm}^{-2} \text{ s}^{-1}$.

Adding a candidate at the position of the BCG in IC 4991 (in the energy band $300 \text{ MeV} \leq E \leq 300 \text{ GeV}$) yields a photon index of 2.379 ± 0.009 and a flux of $(1.64 \pm 0.62) \times 10^{-9} \text{ ph cm}^{-2} \text{ s}^{-1}$. There appear to be two potential non-2FGL sources of γ radiation in the field. For the first, the BCG lies just outside the 95 per cent confidence contour (the fitted peak in TS is located at RA = $304^{\circ}30'$, Dec. = $-41^{\circ}22'$). If this TS peak represents a genuine γ -ray source, it may be associated with the candidate, or perhaps with the *ROSAT* source 1RXS 201731.2–411452, a BL Lac object 6 arcmin removed (Kollatschny et al. 2008). The second TS peak (fit position: RA = $307^{\circ}27'$, Dec. = $-42^{\circ}72'$) may indicate γ -ray emission associated with an 81 mJy SUMSS source 5 arcmin removed that is not clearly identified (see Mauch et al. 2003). Remodelling the data to account for these two sources renders the candidate BCG emission insignificant (reducing the TS to 2.7), and results in a TS of 13.9 for the closer peak, and 41.1 for the peak revealed towards the edge of the field, roughly corresponding to statistical significances of 3.7σ and 6.4σ , respectively. A photon index of 2.2 ± 0.2 and flux of $(8.58 \pm 3.15) \times 10^{-9} \text{ ph cm}^{-2} \text{ s}^{-1}$ is calculated for the significant source.

Table 2 summarizes the detections confirmed after a remodelling to account for sources of γ -ray emission in the three fields described

Table 2. A summary of non-2FGL *Fermi* detections of sources in fields within our sample, giving the fitted position (and error) of the TS peak and the output TS after remodelling the data. No attempt is made to account for trial factors due to the large sample considered, but we note that a TS value of >25 still corresponds to a post-trial significance of $>4\sigma$.

Name	TS ^a	RA ^b (°)	Dec. ^c (°)	Error (°)
FERMI J1350–1140 ^d	179.8	207.33	–11.55	0.11
FGL J0133.0–0758	28.2	23.25	–7.98	0.16
FGL J0127.1–0822	64.8	21.78	–8.37	0.14
FGL J2029.0–4243	41.3	307.27	–42.72	0.22

^aTest Statistic; ^bright ascension; ^cdeclination; ^ddetected by the *Fermi* Large Area Telescope Collaboration in 2011 November (ATel 3788).

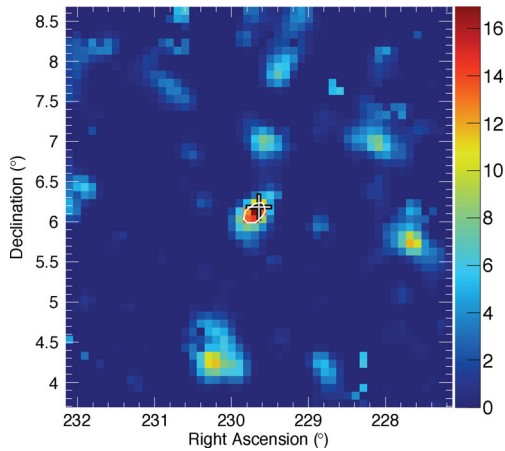


Figure 5. TS map for the candidate source in A2055, produced from $3 \leq E \leq 300$ GeV data. The BCG position is indicated by the central black/grey cross. The 95 per cent confidence contour on the γ -ray source position is shown in white.

above. The TS maps were re-calculated based on the new output models, which were found to describe the emission adequately.

4.3.3 γ -ray emission from A2055

Using the $3 \leq E \leq 300$ GeV data, analysis of the BCG in A2055 (which is classified as a BL Lac object) results in a TS of 15.2. The corresponding TS map is shown in Fig. 5. A hint of emission from the position of the BCG can be clearly seen. The position of the BCG is contained within the 95 per cent confidence region for the source location. With this candidate alone added, the model sufficiently describes the γ -ray emission within the field. The source is not detected in the energy band $30 \leq E \leq 300$ GeV, and the TS drops to 8.0 using the larger $300 \text{ MeV} \leq E \leq 300$ GeV data set.

5 DISCUSSION

There is no statistically significant evidence for emission within the stacked sample. The upper limits derived on an average source within the class of BCGs represent at least an order of magnitude improvement on the individual upper limits presented in Table 1. The derived limits are consistent with the expectation of a $\sim 1/\sqrt{N_{\text{obj}}}$ scaling for the background-limited lower energy bands and $\sim 1/N_{\text{obj}}$ for highest energies where the *Fermi*-LAT becomes signal limited even in the stacked sample, where N_{obj} is the number of fields stacked.

To derive a limit on the γ -ray to radio flux ratio ($F_{1\text{GeV}}/F_{1.4\text{GHz}}$) for the core emission of the sample we consider the *core* radio flux (some fraction of the emission given in Table 1) of each BCG (Hogan et al., in preparation), and find an average radio flux of $2.37 \times 10^{-15} \text{ erg cm}^{-2} \text{ s}^{-1}$ and an average luminosity of $1.8 \times 10^{41} \text{ erg s}^{-1}$ (at an average redshift of 0.13). Given the upper limit on the stacked emission, the average γ -ray flux evaluated at 1 GeV and assuming a photon index of 2 is less than $3.55 \times 10^{-14} \text{ erg cm}^{-2} \text{ s}^{-1}$ and the average γ -ray luminosity is less than $1.35 \times 10^{42} \text{ erg s}^{-1}$. The average $F_{1\text{GeV}}/F_{1.4\text{GHz}}$ of the sample is therefore <15 . The γ -ray flux limit for the sample corresponds to only 0.1 per cent of the flux of NGC 1275, which has $F_{1\text{GeV}}/F_{1.4\text{GHz}} \approx 120$ (~ 90 excluding γ -ray flares). The average core radio flux is ≈ 1 per cent of that of NGC 1275. The lack of a γ -ray signal in the stack therefore implies that the average core-radio selected BCGs have spectral energy distributions with a different shape to that of NGC 1275, with significantly lower γ -ray flux relative to core radio flux, though the current highly variable state of γ -ray emission in this active galaxy (Kataoka et al. 2010) may account for the difference in $F_{1\text{GeV}}/F_{1.4\text{GHz}}$.

NGC 1275 and M87 are the closest cooling-core BCGs, so the detected γ -ray emission is unlikely to be beamed towards us if they are drawn from a random distribution of sight lines. However, a role for beaming in NGC 1275 cannot be excluded and may play a role in its unusual γ -ray brightness (see above). It has been postulated (see Falceto-Gonçalves et al. 2010) that the central AGN comprises a viscous accretion disc tilted with respect to the rotating supermassive black hole, bringing about precessing jets as a result of torques acting on the disc. Very long baseline interferometry (VLBI) maps of the radio source can place constraints on the inclination of the system; to be satisfied, some curvature of the jet away from the line of sight is implied (Dunn, Fabian & Sanders 2006). This said, for those BCGs with bona fide BL Lac nuclei, for example A2055 and A3392, which are significantly more distant and comparable to most of the parent sample, the probability of observing a few sources close to the jet direction is significant.

We can assess the number of local clusters hosting a *Fermi*-LAT AGN by cross-correlating the Abell cluster catalogue of 5250 clusters (including the supplementary systems; Abell, Corwin & Olowin 1989) with the 2FGL. Of the 85 coincidences within 20 arcmin, only 11 are consistent with the 2FGL source being a cluster member and of those only four being the BCG (NGC 1275 in A426/Perseus, PKS 0625–35 in A3392, PKS 2035–714 in A3701 and PKS 2316–423 in S1111). The latter two clusters are not detected above the X-ray flux limit for the eBCS or REFLEX catalogues, so were not considered in the analysis above. Therefore, the chance of finding a *Fermi* source in any particular cluster is relatively small but is significant.

The added complication with the analysis is that the *Fermi*-LAT spatial resolution and source density ($\approx 0.05 \text{ deg}^{-2}$) implies chance coincidences of the order of a few when more than 100 positions are considered. This is illustrated in Fig. 4, given that the TS output from the initial binned likelihood analysis of the field was in each case not exclusively associated with the BCG under scrutiny, but a nearby source of emission not described by the model. The angular resolution of the *Fermi*-LAT is sufficient (particularly above 1 GeV) to isolate nearby background sources from the position of interest in most cases, but the likelihood analysis is not robust enough to accurately disentangle the γ emissions in such an event.

Four *detections* (i.e. of TS > 25 emission) have been made of sources not contained in the 2FGL (see Table 2). For those above a TS of ~ 50 , their absence from the 2FGL implies temporal

variability in the emission, as appears to be the case for the source FERMI J1350–1140. A more detailed study of these sources is left to future work. The tentative evidence for emission from the BCG in A2055 will be refuted or validated in time; if the significance of emission from the source position continues to increase, it will be the fourth such source to be detected using *Fermi*, and the second BCG hosting a BL Lac.

6 CONCLUDING REMARKS

The *Fermi*-LAT detection of a few sources in clusters of galaxies sets important limits on the energetics and emission mechanisms at work in the cores of the most massive member galaxies. The detections of BCGs using *Fermi* are strongly biased towards the most radio-bright systems or those that are dominated by a beamed core. Our statistical upper limit from a larger sample of sources with lower radio flux indicates that the average core-radio selected BCG is more than an order of magnitude less γ -ray luminous than for example NGC 1275. Furthermore, the ratio of γ -ray to radio flux is <15 , compared with $F_{1\text{GeV}}/F_{1.4\text{GHz}} \approx 120$ for NGC 1275. The BCG in A2055, which hosts a BL Lac, may soon be detectable in HE γ -rays (given a longer exposure using *Fermi*), and if so will corroborate this conclusion.

Detections of a number of new sources are declared; though none of these appear to be unambiguously associated with the BCG, the slightly offset emission in the field of RXC J0132.6–0804 might be associated with the candidate, or else another cluster member galaxy, and in the field of IC 4991 may (if genuine) in part originate from the BCG. This work also illustrates, then, the need to carefully assess all the possible sources of emission that could explain the *Fermi*-LAT detections found in clusters before attributing them to e.g. cluster merger-related shocks or DM annihilation.

ACKNOWLEDGMENTS

The authors would like to thank Stefan Ohm for useful comments and discussions. This work has made use of public *Fermi* data and Science Tools provided by the *Fermi* Science Support Centre. K. L. Dutton and R. J. White acknowledge support from the STFC and J. A. Hinton from the Leverhulme Trust.

REFERENCES

Abdo A. A. et al., 2009a, *ApJ*, 699, 31
 Abdo A. A. et al., 2009b, *Phys. Rev. D*, 80, 122004
 Abell G. O., Corwin H. G. Jr, Olowin R. P., 1989, *ApJS*, 70, 1
 Abramowski A. et al., 2012, *ApJ*, 746, 151
 Ackermann M. et al., 2010a, *J. Cosmol. Astropart. Phys.*, 5, 25
 Ackermann M. et al., 2010b, *ApJ*, 717, L71
 Aharonian F. A., 2002, *MNRAS*, 332, 215
 Aharonian F. et al., 2006, *Sci*, 314, 1424
 Aleksić J. et al., 2012, *A&A*, 539, L2
 Antonucci R., 1993, *ARA&A*, 31, 473
 Asada K., Kameno S., Shen Z.-Q., Horiuchi S., Gabuzda D. C., Inoue M., 2006, *PASJ*, 58, 261
 Atwood W. B. et al., 2009, *ApJ*, 697, 1071
 Benson A. J., Bower R. G., Frenk C. S., Lacey C. G., Baugh C. M., Cole S., 2003, *ApJ*, 599, 38
 Biretta J. A., Stern C. P., Harris D. E., 1991, *ApJ*, 101, 1632

Blasi P., Colafrancesco S., 1999, *Nucl. Phys. B: Proc. Suppl.*, 70, 495
 Blasi P., Gabici S., Brunetti G., 2008, *Int. J. Modern Phys. A*, 22, 681
 Böhringer H. et al., 2004, *A&A*, 425, 367
 Bower R. G., Benson A. J., Malbon R., Helly J. C., Frenk C. S., Baugh C. M., Cole S., Lacey C. G., 2006, *MNRAS*, 370, 645
 Brown M., Adams J., 2012, *MNRAS*, 413, 2785
 Burns J. O., 1990, *AJ*, 99, 14
 Cavagnolo K. W., Donahue M., Voit G. M., Sun M., 2008, *ApJ*, 683, L107
 Clarke T. E., Sarazin C. L., Blanton E. L., Neumann D. M., Kassim N. E., 2005, *ApJ*, 625, 748
 Condon J. J., Cotton W. D., Greisen E. W., Yin Q. F., Perley R. A., Taylor G. B., Broderick J. J., 1998, *AJ*, 115, 1693
 Dunn R. J. H., Fabian A. C., Sanders J. S., 2006, *MNRAS*, 366, 758
 Ebeling H., Edge A. C., Böhringer H., Allen S. W., Crawford C. S., Fabian A. C., Voges W., Huchra J. P., 1998, *MNRAS*, 301, 881
 Ebeling H., Edge A. C., Allen S. W., Crawford C. S., Fabian A. C., Huchra J. P., 2000, *MNRAS*, 318, 333
 Ebeling H., Edge A. C., Henry J. P., 2001, *ApJ*, 553, 668
 Edge A. C., Stewart G. C., Fabian A. C., Arnaud K. A., 1990, *MNRAS*, 245, 559
 Fabian A. C., 1994, *ARA&A*, 32, 277
 Fabian A. C. et al., 2000, *MNRAS*, 318, L65
 Fabian A. C., Allen S. W., Crawford C. S., Johnstone R. M., Morris R. G., Sanders J. S., Schmidt R. W., 2002, *MNRAS*, 332, L50
 Falceto-Gonçalves D., de Gouveia Dal Pino E. M., Gallagher J. S., Lazarian A., 2010, *ApJ*, 708, L57
 Hinton J. A., Domainko W., Pope E. C. D., 2007, *MNRAS*, 382, 466
 Hlavacek-Larrondo J., Fabian A. C., Sanders J. S., Taylor G. B., 2011, *MNRAS*, 415, 3520
 Huber B., Farnier C., Manalaysay A., Straumann U., Walter R., 2012, *A&A*, 547, 102
 Jackson C. A., Wall J. V., Shaver P. A., Kellermann K. I., Hook I. M., Hawkins M. R. S., 2002, *A&A*, 386, 97
 Kataoka J. et al., 2010, *ApJ*, 715, 554
 Kollatschny W., Kotulla R., Pietsch W., Bischoff K., Zetzl M., 2008, *A&A*, 484, 897
 McNamara B. R., Nulsen P. E. J., 2007, *ARA&A*, 45, 117
 McNamara B. R. et al., 2000, *ApJ*, 534, L135
 Mattox J. R. et al., 1996, *ApJ*, 461, 396
 Mauch T., Murphy T., Buttery H. J., Curran J., Hunstead R. W., Piestrzynski B., Robertson J. G., Sadler E. M., 2003, *MNRAS*, 342, 1117
 Mittal R., Hudson D. S., Reiprich T. H., Clarke T., 2009, *A&A*, 501, 835
 Nolan P. L. et al., 2012, *ApJS*, 199, 31
 Paggi A., Massaro F., D'Abrusco R., 2012, *Astron. Telegram*, 4086, 1
 Peterson J. R., Kahn S. M., Paerels F. B. S., Kaastra J. S., Tamura T., Bleeker J. A. M., Ferrigno C., Jernigan J. G., 2003, *ApJ*, 590, 207
 Pfrommer C., Enßlin T. A., 2004, *A&A*, 413, 17
 Plotkin R. M., Anderson S. F., Hall P. B., Margon B., Voges W., Schneider D. P., Stinson G., York D. G., 2008, *ApJ*, 135, 2453
 Rolke W. A., López A. M., Conrad J., 2005, *Nucl. Instrum. Methods Phys. Res. A*, 551, 493
 Russell H. R., Fabian A. C., Sanders J. S., Johnstone R. M., Blundell K. M., Brandt W. N., Crawford C. S., 2010, *MNRAS*, 402, 1561
 Sijacki D., Springel V., Di Matteo T., Hernquist L., 2007, *MNRAS*, 380, 877
 Sparks W. B., Biretta J. A., Macchetto F., 1996, *ApJ*, 473, 254
 Torresi E., D'Ammando F., 2011, *Astron. Telegram*, 3788, 1
 Vermeulen R. C., Readhead A. C. S., Backer D. C., 1994, *ApJ*, 430, 41
 Völk H. J., Atoyan A. M., 1999, *Astropart. Phys.*, 11, 73
 Wise M. W., McNamara B. R., Nulsen P. E. J., Houck J. C., David L. P., 2007, *ApJ*, 659, 1153

This paper has been typeset from a $\text{\TeX}/\text{\LaTeX}$ file prepared by the author.